Structural Evidence for a Ligand Coordination Switch in Liver Alcohol Dehydrogenase[†]

Rob Meijers,*,‡,§ Hans-Werner Adolph,‖ Zbigniew Dauter,⊥ Keith S. Wilson,@ Victor S. Lamzin,‡ and
Eila S. Cedergren-Zeppezauer*,#

*European Molecular Biology Laboratory, Hamburg Outstation, c/o DESY, Notkestrasse 85, D-22603 Hamburg, Federal
Republic of Germany, Organic Macromolecular Chemistry, Postfach 151150, Saarland University, D-66041 Saarbrücken,
Federal Republic of Germany, Synchrotron Radiation Research Section, MCL, NCI, Argonne National Laboratory, Argonne,
Illinois 60439, York Structural Biology Laboratory, Department of Chemistry, University of York, Heslington, York YO10 5YW,
U.K., and Department of Biochemistry, Centre for Chemistry and Chemical Engineering, Lund University, P.O. Box 124,
SE-22100 Lund, Sweden*

ABSTRACT: The use of substrate analogues as inhibitors provides a way to understand and manipulate enzyme function. Here we report two 1 Å resolution crystal structures of liver alcohol dehydrogenase in complex with NADH and two inhibitors: dimethyl sulfoxide and isobutyramide. Both structures present a dynamic state of inhibition. In the dimethyl sulfoxide complex structure, the inhibitor is caught in transition on its way to the active site using a flash-freezing protocol and a cadmium-substituted enzyme. One inhibitor molecule is partly located in the first and partly in the second coordination sphere of the active site metal. A hydroxide ion bound to the active site metal lies close to the pyridine ring of NADH, which is puckered in a twisted boat conformation. The cadmium ion is coordinated by both the hydroxide ion and the inhibitor molecule, providing structural evidence of a coordination switch at the active site metal ion. The structure of the isobutyramide complex reveals the partial formation of an adduct between the isobutyramide inhibitor and NADH. It provides evidence of the contribution of a shift from the keto to the enol tautomer during aldehyde reduction. The different positions of the inhibitors further refine the knowledge of the dynamics of the enzyme mechanism and explain how the crowded active site can facilitate the presence of a substrate and a metal-bound hydroxide ion.

Zn-dependent medium chain dehydrogenases/reductases (MDRs)[1] belong to a large family of NAD/NADP-dependent enzymes, which are ubiquitous among all species (*1*). These enzymes catalyze the transfer of a hydride ion between a red–ox pair consisting of NAD(H)/NADP(H) and a great variety of substrates. The substrates are most often part of a metabolic pathway, and inhibition of an enzyme can cause organisms to switch pathways or build up metabolic intermediates (*2*). Furthermore, NAD/NADP plays a role as a signaling molecule, and in this case, enzyme inhibition affects the response of the organism to changes in its environment. X-ray structures of a number of Zn-dependent MDRs show that they share a common structural architecture first described for horse liver alcohol dehydrogenase (LADH) (*3*). All enzymes in this group contain a NAD(P) binding domain that is shaped as a Rossmann fold (*4*), with an active site zinc ion and a substrate binding pocket. The substrate binding channel varies considerably in size and defines diverse specificity. Thus, there is a wide variety in substrates, assemblies of enzyme subunits, and temperature stabilities (*5*). The reaction mechanism centers on the zinc ion bound deep inside these enzymes. The zinc ion is liganded by three or four amino acids in a varying combination of cysteine, histidine, and glutamic acid residues. Metal–ligand coordination at the active center varies between members among the MDRs, but the hydride transfer reaction between the zinc-bound substrate and the pyridine ring of the cofactor is a general feature.

In the active site of LADH, zinc is coordinated by C46, H67, and C174. Kinetic studies (*6*) indicate that a water molecule or hydroxide ion is bound to the active site zinc ion as a fourth ligand in the apoenzyme as well as in the binary complex with NAD(H). X-ray structures of ternary complexes of LADH with NAD(H) and substrate analogues show the analogue is bound to the active site metal ion as a fourth ligand replacing the water molecule (*7, 8*). A fundamental question in MDR enzymology is whether and how the water molecule or hydroxide ion is replaced by the substrate as a metal ligand. On the basis of geometrical considerations derived from the X-ray structures, it was

concluded that the active site metal ion is restricted to coordinate four ligands (*9*). Spectroscopic data, however, indicate the presence of a pentacovalent intermediate, where both the substrate and the water molecule or hydroxide ion are simultaneously bound to the metal (*10, 11*).

Atomic-resolution structures of LADH in complex with NADH and 2-methyl-2,4-pentanediol (MPD) showed that a hydroxide ion may form an adduct with the nicotinamide of NADH (*12*). In those structures, MPD binds to the binary NADH complex and represents a stable, abortive complex with the alcohol ligand situated in the second coordination sphere of the zinc ion. However, MPD does not mimic the presence of an aldehyde substrate. We therefore turned to the substrate analogue dimethyl sulfoxide (DMSO), which inhibits the enzyme by binding to the metal ion in the presence of NADH (*13*), to see whether the displacement of the hydroxide ion is indeed triggered by the approaching substrate.

Two measures to slow the binding of the inhibitor to the enzyme to capture an intermediate state were taken. First, the active zinc ion was replaced with cadmium, which results in an enzyme that is two orders of magnitude less active (*14*). Second, a cadmium-substituted LADH−NADH crystal with a MPD molecule near the active site was soaked in a solution with the inhibitor DMSO and flash-frozen immediately. The flash-frozen crystal diffracted to 1.0 Å resolution, and we observed the inhibitor on its way to block the active site in two conformations. To further the picture of inhibition, we collected atomic-resolution data on a NADH complex containing the strong inhibitor isobutyramide (IBA) (*15*). In this structure, the cofactor−water interaction with the active site zinc ion is broken, and the hydroxide ion is totally removed from the active site. We compare these structures with those containing MPD at the same high resolution, and the previously determined structure of a LADH−NADH complex with DMSO (*8*). The comparison contributes further evidence of the involvement of a hydroxide ion in catalysis, and it provides a detailed picture of the inhibition of aldehyde reduction.

EXPERIMENTAL PROCEDURES

Preparation of the Enzyme. Dimeric Zn-LADH (EC 1.1.1.1), the "EE-isozyme", was prepared according to procedures described previously (*16*). A sample of the enzyme was prepared in such a way that the native zinc metal (four atoms per molecule) was replaced with cadmium at two catalytic sites and two noncatalytic centers (Cd$_4$) (*17*). The metal content was determined by atomic absorption spectroscopy in flame mode (Perkin-Elmer 2100 atomic absorption spectrometer), indicating the presence of 2.0 ± 0.1 Cd^{2+} ions per subunit and fewer than 0.2 Zn^{2+} ion per subunit.

Preparation of Crystalline LADH−NADH Complexes. The Cd-LADH−NADH species forms a complex with MPD similar to that with Zn-LADH, and the structure of the resulting complex has been published previously [PDB entry 1HEU (*18*)] (*12*). It is here called Cd-MPD−NADH for comparison. It crystallizes under conditions similar to those of the native Zn-bound enzyme in high concentrations of MPD. A crystal of the Cd-MPD-NADH complex was soaked in a cryoprotectant containing 25% PEG 400 and 20%

Table 1: X-ray Data Statistics of Alcohol Dehydrogenase−Cofactor Complexes[a]

	Cd-DMSO−NADH	Zn-IBA−NADH
PDB entry	2JHF	2JHG
EMBL (DESY) beamline	BW7B	X11
detector	MAR Imaging Plate	Mar CCD
temperature (K)	120	100
space group	*P*1	*P*1
unit cell dimensions		
a, *b*, *c* (Å)	50.87, 44.46, 94.18	50.19, 43.80, 92.52
α, β, γ (deg)	104.4, 101.4, 71.1	102.9, 92.6, 71.1
resolution (Å)	25.0−1.0 (1.03−1.00)	25.0−1.20 (1.23−1.20)
no. of measured reflections	540964	552610
no. of unique reflections	323884	212570
completeness (%)	80.0 (67.5)	94.1 (89.1)
$I/\sigma(I)$	16.7 (1.4)	17.8 (2.8)
R_{merge}[b] (%)	4.3 (43.9)	5.0 (22.5)
no. of waters	1242	1236
no. of protein residues (with double conformations)	748 (51)	748 (101)
R_{factor}[c] (%)	12.5	11.5
R_{free}[d] (%)	15.2	14.2
DPI[e] (Å)	0.07	0.03

[a] Numbers in parentheses refer to the outer (highest) resolution shell. [b] $R_{merge} = \sum\sum|I_i - \langle I \rangle|/\sum\sum(I)$, where I_i is the intensity for the *j*th measurement of a reflection with indices *hkl* and $\langle I \rangle$ is the weighted mean of the reflection intensity. [c] $R_{factor} = \sum F_o(hkl) - F_c(hkl)/\sum F_o(hkl)$, where F_o and F_c are the observed and calculated structure factor amplitudes, respectively. [d] R_{free} is the crystallographic R_{factor} calculated with 0.4% of the data that were excluded from the structure refinement. [e] Cruickshank's diffraction precision index (*43*).

dimethyl sulfoxide (DMSO). X-ray data for Cd-DMSO−NADH were collected to 1.0 Å resolution (Table 1).

Zn-LADH forms a strong complex with isobutyramide (IBA) in the presence of NADH (but not NAD$^+$). The constant for dissociation of NADH from the complex is 5 × 10^{-9} M (*15*). The ternary inhibitor complex was formed in solution, with 25 mg/mL LADH, 100 mM IBA, and 0.7 mM NADH. Crystals were obtained by dialysis in a buffer solution of 30 mM Tris-HCl (pH 8.2), and the final precipitant concentration was 25% (v/v) MPD. PEG 400 (30%, v/v) was added as a cryoprotectant. The complex is termed Zn-IBA−NADH (Table 1).

Data Collection and Refinement. All X-ray data were collected on the synchrotron beamlines at the EMBL Hamburg Unit at DESY using a MAR Research imaging plate or a CCD detector. Crystals were flash-frozen in an air stream at liquid nitrogen temperature using an Oxford Cryo System. A single crystal was used to collect data for each complex. Both structures belong to space group *P*1 with a dimeric molecule in the asymmetric unit. X-ray data were processed, merged, and scaled with the HKL program suite (*19*). The structure of PDB entry 1HET determined at 1.15 Å resolution was used as a starting model (*12*).

The structures were refined with SHELX-97 (*20*) and REFMAC5 (*21*). Manual correction was done with Xtalview (*22*), and ARP/wARP (*23*) was used to build the solvent model. The refinement protocol included a bulk solvent correction, the use of anisotropic displacement parameters for each individual non-hydrogen atom, and hydrogen atoms

were included at their idealized positions. The geometrical restraints were modified for residues in the neighborhood of the active site to fit best the observed electron density. This included a relaxation of restraints on the nicotinamide of the NADH molecule, as well as the removal of antibumping restraints on the metal site. Table 1 lists the refinement statistics. Superposition of the models was performed with LSQKAB (*24*), and figures were prepared with PyMol (*25*). The recorded X-ray structure factor amplitudes and the derived atomic coordinates have been deposited in the Protein Data Bank as entries 2JHF and 2JHG.

RESULTS

Displacement of the MPD Molecule by DMSO in the Active Site of LADH. In all the NADH−LADH crystal structures presented here, the enzyme is in a "closed" conformation with NADH bound in the coenzyme binding cleft. Cd-LADH is an active enzyme (*14*), and the deviations in catalytic behavior from that of the native enzyme have been attributed to the larger Cd ion radius. As expected, the Cd^{2+}−ligand bonds are on average ∼0.2 Å longer than the Zn^{2+}−ligand bonds. The backbone structure of the Cd-DMSO−NADH complex is almost identical to the Cd-MPD−NADH complex reported earlier [PDB entry 1HEU (*12*)]. The root-mean-square deviation (rmsd) for all 748 Cα atoms is only 0.12 Å. The main systematic deviations observed in both monomers concern residues 116−120 and 294−300. The first region is situated near the substrate binding channel. The difference in conformation occurs due to an interaction between the side chain of L116 and the secondary alcohol group of the MPD molecule in the Cd-MPD−NADH structure (Figure 1). The side chain thus shields the MPD molecule from its polar surroundings, and this interaction may in fact contribute substantially to the binding energy of the MPD molecule, which does not coordinate to the metal. In the Cd-DMSO−NADH−LADH complex, the L116 side chain swings away from the substrate channel and occupies the binding site previously occupied by the secondary alcohol group of MPD. A water molecule at full occupancy emerges in the area formerly occupied by the L116 side chain. This water molecule (WL in Figure 1) is located 10 Å from the metal ion and has been observed previously (*8*). LADH can oxidize alcohols with aliphatic tails, and L116 may contribute to the channeling of the substrate to the active site. In the steroid specific form of LADH, the region from residue 116 to 120 is truncated and relocated to allow bulkier substrates to enter the substrate-binding groove (*26*).

The second region spanning residues 294−300 is situated near the proton relay cascade (*27*) consisting of S48, H51, and the ribose unit of the nicotinamide moiety. The main differences between the Cd-DMSO−NADH and Cd-MPD−NADH structures concern residues V294 and P295, and there is a substantial shift in the position of the carbonyl oxygen of V294. In the MPD complexes of both the native and cadmium-substituted enzymes, this carbonyl oxygen is close to H51, and the distance between NE2 of H51 and the carbonyl oxygen ranges between 3.38 Å for subunit A and 3.46 Å for subunit B. The C−O−NE2 angle is 136°, which qualifies this interaction as a weak hydrogen bond. In the Cd-DMSO−NADH complex, this distance is increased to 3.88−3.92 Å with a more unfavorable C−O−NE2 angle of
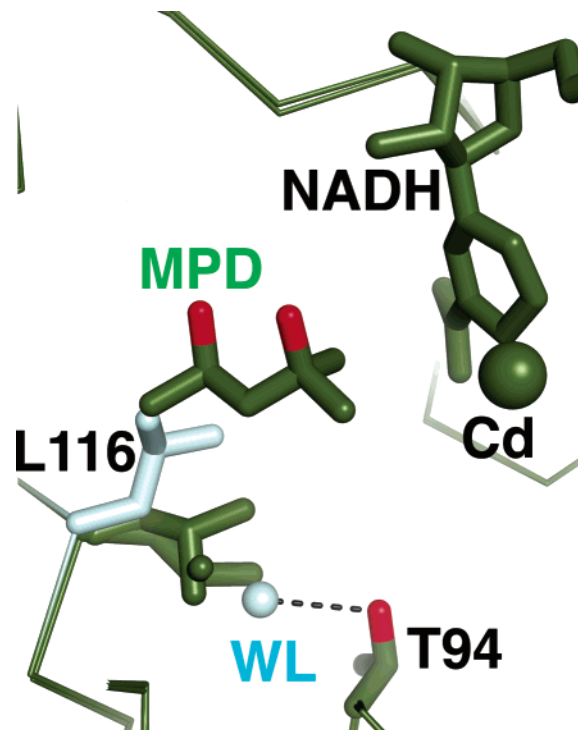

FIGURE 1: Comparison between the conformations of L116 in the Cd-MPD−NADH complex (green) and the Cd-DMSO−NADH complex (light gray) after MPD has been expelled. The Cα trace is displayed as a ribbon, and the L116 and T94 side chains, as well as the MPD and NADH molecules, are rendered as sticks. The active site metal (Cd) and a water molecule (WL) are shown as spheres.

130° for both subunits, therefore breaking this weak hydrogen bond. The NE2 atom on H51 is thought to provide a proton to the ribose unit of the nicotinamide, which is then transferred to the aldehyde substrate through S48 (*28*). Kinetic studies on the NAD^+−enzyme complex indicate the proton relay system controls the formation of the ternary complex (*29*). The enzyme undergoes a change from an open to a closed conformation while switching from an apo state to a binary and ternary complex. The region of residues 294−300 is essential in the transformation from an open to a closed conformation (*30*), and the interaction between H51 and V294 provides a structural switch whereby the proton relay system controls the formation of the ternary complex.

DMSO acts as a weak inhibitor ($K_i = 1.5$ mM) (*7*) and is regarded as an aldehyde/ketone substrate analogue. The active site of the Cd-DMSO−NADH structure contains one DMSO molecule in two alternate conformations in both subunits. One conformation with an occupancy of 50% situates the DMSO molecule in the second coordination sphere with the oxygen atom 5.6 Å from the metal (Figure 2a). It occupies roughly the same area as the tertiary alcohol side of the MPD molecule in the Cd-MPD−NADH structure (see Figure 1 for comparison).

The other conformation with an occupancy of 50% corresponds to the end state inhibition complex (Figure 2b), where the oxygen is coordinated to the active site metal, as previously observed in the Zn-DMSO−NADH structure (*8*). This conformation displaces the "substrate site" metal-bound water molecule (WS) seen in the Cd-MPD−NADH structure. The most striking feature in the Cd-DMSO−NADH structure is the presence of a hydroxide ion close to the nicotinamide
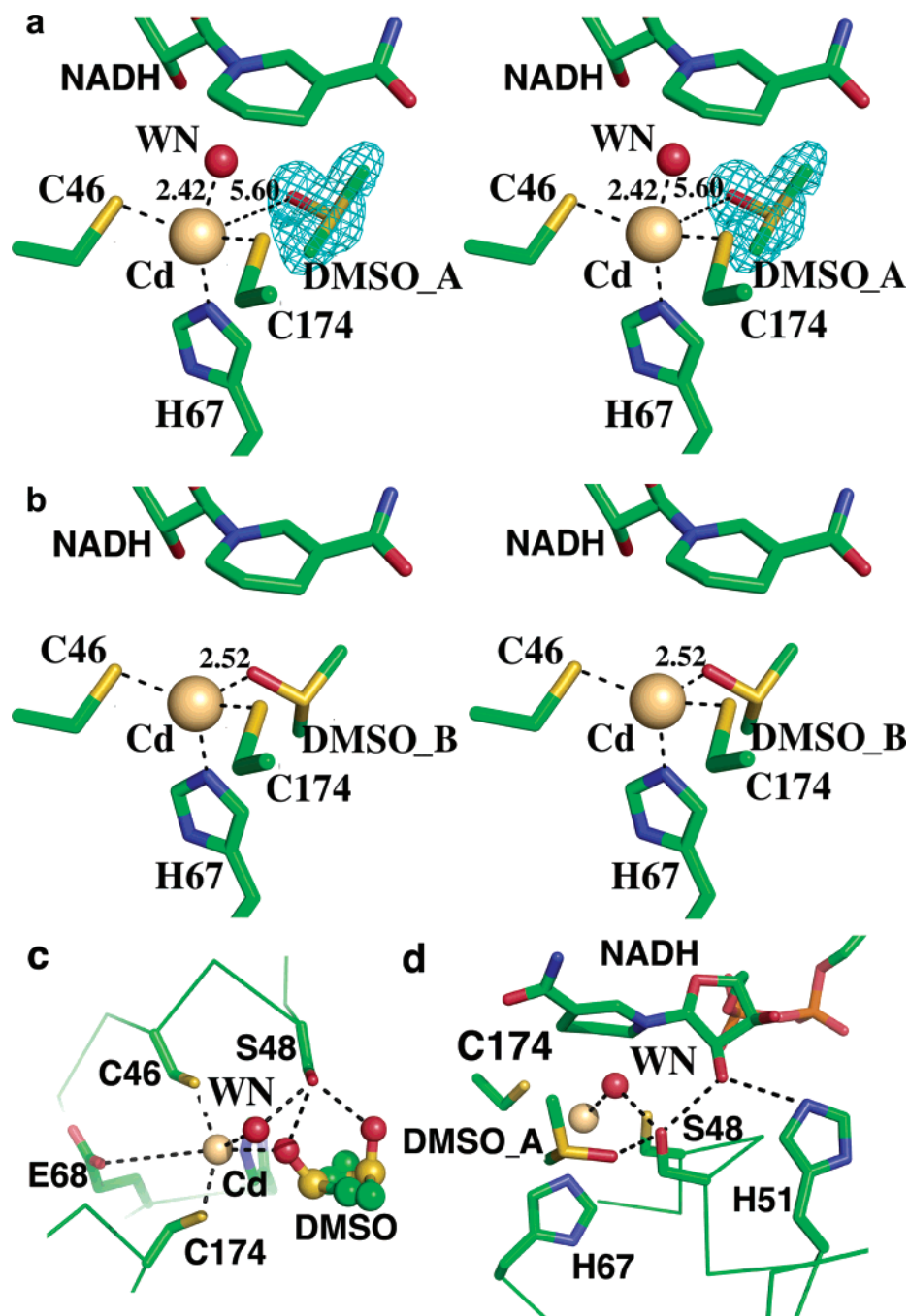
FIGURE 2: Active site of the Cd-DMSO−NADH complex. (a) Stereoview of the ligand coordination around the active site cadmium ion with the protein ligands. The DMSO molecule is in the conformation most distant from the active site metal (DMSO_A). The NADH and DMSO molecules are displayed as sticks and the cadmium and hydroxide ion (WN) as spheres. An omit map colored cyan at the 3.5σ (0.24 e/Å^3) contour level is shown for the unusual DMSO conformation. Distances are shown between the active site metal and the hydroxide ion as well as the remote DMSO molecule (DMSO_A). (b) Stereoview of the second coordination conformation with the DMSO molecule liganded to the active site metal (DMSO_B). The hydroxide ion is no longer present. (c) Hydrogen bonding network around S48, involving both DMSO conformations as well as the hydroxide ion (WN). The nicotinamide ring is omitted for clarity. (d) Proton relay cascade consisting of the remote DMSO conformation (DMSO_A), the hydroxide ion, S48, the ribose of the nicotinamide moiety, and H51.

ring (WN in Figure 2a). It is situated in the same position that was observed for the Zn/Cd-MPD−NADH complexes (*12*). The occupancy of the second conformation of the DMSO molecule and the hydroxide ion is similar (50%). The hydroxide ion acts as the fourth ligand of the cadmium ion when the DMSO molecule is not yet coordinated. The hydroxide ion is only 1.7 Å from the end state conformation of the DMSO molecule, and the distance between the hydroxide ion and the oxygen of the second DMSO conformer is 4.2 Å. A complete list of metal−ligand

distances and angles for the first coordination sphere of the metal is given in Table S1 of the Supporting Information.

A key residue in the shuttling of the DMSO molecule toward the metal ion is S48 (Figure 2c,d). It is thought to be the residue that shuttles a proton to and from the active site. The side chain hydroxyl group of S48 is almost equidistant from the oxygen of both DMSO conformations (2.6 Å for the end state and 2.7 Å for the approaching conformation), as well as the metal-bound hydroxide ion WN (2.6 Å). Despite the complex interactions involving this side chain,
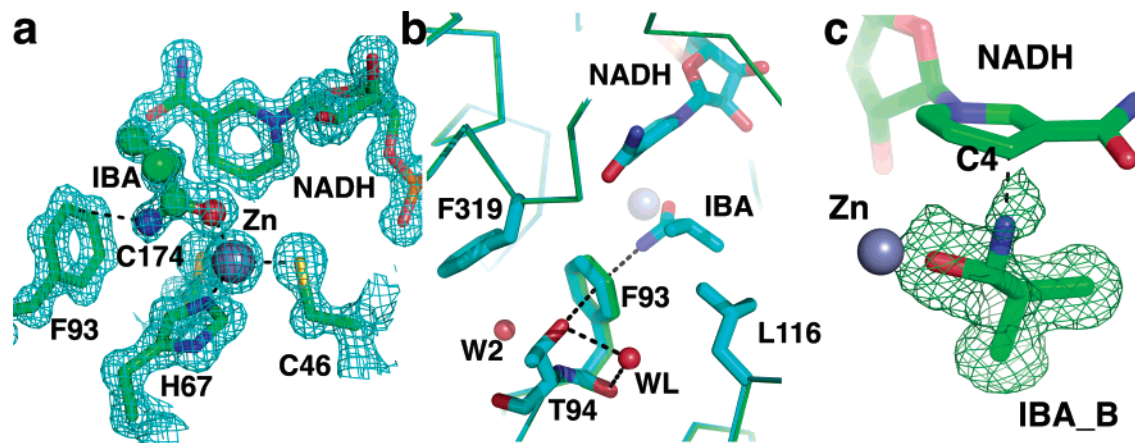
FIGURE 3: Active site of the Zn-IBA−NADH−LADH complex. (a) Ligand coordination around the active site zinc ion with protein ligands, IBA, and the NADH molecule displayed as sticks. A $2mF_o − DF_c$ electron density map is displayed at a 2σ contour level (0.89 e/Å^3). (b) π-H interaction between IBA and F93, which affects the hydrogen bonding network of the water molecule unique for inhibitor complexes (WL), as well as the interactions of water molecule W2 located between F93 and Phe319. (c) Formation of a partial adduct between IBA and the C4 atom on the pyridine ring of NADH. An omit density map at the 1.5σ contour level (0.11 e/Å^3) is displayed for the IBA$_B$ adduct.

the electron density is clear and there is only a single conformation.

Isobutyramide Interactions. The structure of isobutyramide (IBA) in complex with the native enzyme with NADH bound (Zn-IBA−NADH) superimposes on Zn-MPD−NADH (PDB entry 1HET) with a rmsd of 0.31 Å for all Cα atoms in the dimer. The only region that differs more than twice the rmsd in both subunits contains V294 and P295. The carbonyl oxygen of V294 is situated 3.5 Å (3.4 Å in the second subunit) from the NE2 atom of H51, similar to the distance in MPD complexes. An isobutyramide molecule is found in a position very similar to the end state position of the DMSO molecule. The carboxyl oxygen atom of IBA forms a bond with a length of 2.1 Å with the zinc ion. Compared to the MPD complex, the water/hydroxide ion is eliminated from the first coordination sphere (Figure 3a). No MPD molecule is detected in the active site of the IBA complex. The amide group of IBA is directed toward F93, interacting with the phenyl ring at a short distance (3.1 Å from the CE atom and 3.2 Å from the CZ atom). A similar π−H-bond interaction was reported for ternary complexes with NADH and formamides (*31*). The aromatic ring of F93 is pushed away, even when the van der Waals restraints on the carbon atoms of the aromatic ring of F93 are removed. A water molecule (W2), which is always present in native LADH structures on the other side of the aromatic ring between F93 and F319 (Figure 3b), is not displaced upon IBA binding. More important though is the π−H-bond interaction between F93 and T94. The displacement of the aromatic ring of F93 moves the CE1 atom from 3.4 Å to within 3.2 Å of the OG1 atom of T94. This directly influences the hydrogen bonding network of the spare water molecule (WL in Figures 1 and 3b) 10 Å from the active site metal, which also forms a hydrogen bond with the OG1 atom of T94. This water molecule occurs in both the DMSO and IBA structures in which the inhibitors coordinate to the active site metal and deplete the site of water/hydroxide but is absent in the MPD complexes in which no substrate analogue is coordinating to the metal to replace the water/hydroxide. Alanine substitution of F93 established it is not essential for catalysis,

although the inhibition by bulky substrate analogues with amide groups is weakened when F93 is substituted (*31*).

When the IBA molecule is fitted into the electron density at full occupancy, there is residual electron density left between the IBA molecule and the nicotinamide, and negative density occurs around the amide group. Figure 3c shows the residual density when it is modeled as a keto form at 60% occupancy, indicating there is clearly electron density between the nicotinamide and the IBA molecule. A second molecule was modeled in the density with 40% occupancy. Here the amide group forms an adduct with the C4 atom of the pyridine ring at a distance of 1.9 Å, and the angle between the nitrogen and oxygen atom of the IBA molecule has to be decreased to 109° to bring the nitrogen atom into the density and close to the C4 atom of the nicotinamide. Consequently, the tetrahedral geometry of the central C1 atom of the IBA molecule indicates that the double bond of the carbonyl group is broken.

Puckering of the Nicotinamide Pyridine Ring. In the structures of the Zn/Cd-MPD−NADH complex at 1 Å resolution, the pyridine ring is puckered in a twisted boat conformation, and this may well mimic the transition state conformation for hydride transfer (*12*). In the Cd-DMSO−NADH complex structure presented here, the pyridine ring has a twisted boat conformation similar to the Zn/Cd-MPD−NADH structures (Table 2). In the Zn-IBA−NADH structure as well as in a number of other reported structures (Table 2), the twist has essentially disappeared. When the pyridine ring puckering between the DMSO and IBA complexes presented here is compared (Figure 4a), it appears that the only deformation occurs at the C5 position of the ring. Moreover, when the electron density is contoured at a level that displays the core electron density distribution around the atoms of the ring, one sees a shift in distribution between the twisted and plain boat conformation. In the plain boat conformation, the electron density is evenly distributed around the ring (Figure 4b). In the twisted boat conformation, the distribution is localized with increased density along the N1−C2 and C4−C5 bonds (Figure 4c). The redistribution of electron density from an even distribution, where the

Table 2: Comparison of the Puckering Parameters of NADH for Relevant LADH−NADH Complexes

complex (subunit)		resolution (Å)	α_C (deg)[d]	α_N (deg)[d]	twist (Å)	reference
Cd-MPD−NADH	subunit A	1.15	13.4	12.3	−0.3	1HEU
Cd-MPD−NADH	subunit B		11.9	14.8	−0.4	
Cd-DMSO−NADH[a]	subunit A	1.00	13.0	13.3	−0.3	2JHF
Cd-DMSO−NADH	subunit B		17.4	13.3	−0.3	
Zn-(MPD)−NADH	subunit A	1.10	9.2	4.9	−0.5	1HET
Zn-(MPD)−NADH	subunit B		10.5	3.0	−0.6	
Zn-IBA−NADH	subunit A	1.20	13.2	12.0	0.0	2JHG
Zn-IBA−NADH	subunit B		10.2	14.6	−0.1	
Zn-PYR−NAD[b]	subunit A	1.13	26.4	13.2	0.0	1N8K
	subunit B		31.0	10.0	0.1	
Zn-DMSO−NADH[c]	subunit A	1.80	19.0	11.1	0.0	2OHX
Zn-DMSO−NADH	subunit B		16.4	11.7	0.0	

[a] Parameters of the dynamic complex between DMSO and the cadmium-substituted enzyme, with a hydroxide ion present in the active site. [b] These parameters were derived from a tertiary complex structure of Zn-LADH showing a NAD−pyrazole derivative (39). [c] Parameters of the end state inhibitor complex between the native enzyme and DMSO (8). [d] Puckering parameters for the pyridine ring (12), where α_N is the angle between the planes of atoms N1−C2−C6 and C2−C3−C6 of the pyridine ring; α_C is the angle between the planes of atoms C3−C4−C5 and C2−C3−C6. The twist is the shortest distance between the C5 atom and the plane formed by atoms C2−C3−C6.
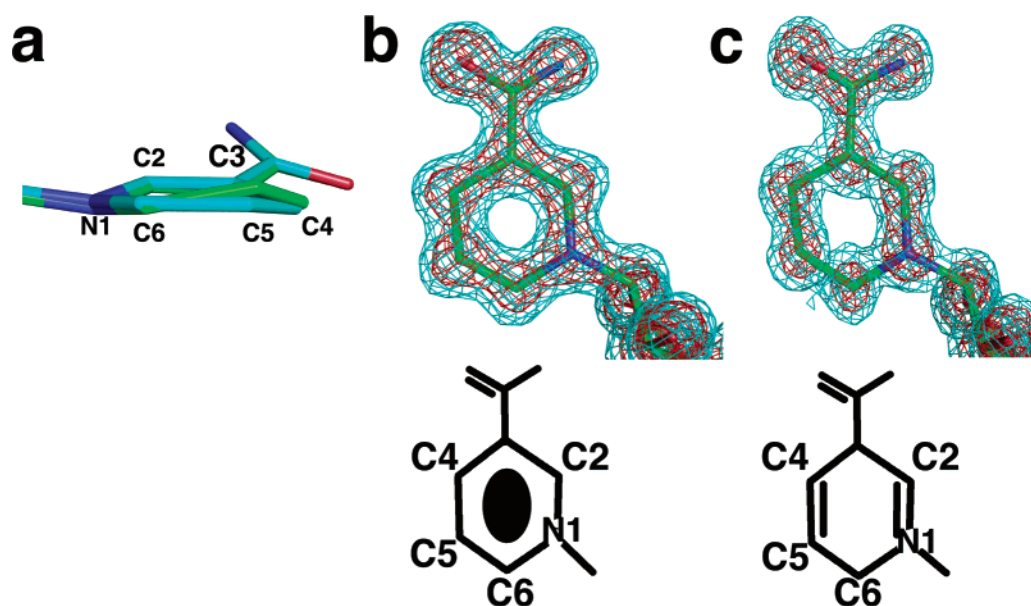

FIGURE 4: Pyridine ring puckering in the nicotinamide moiety of NADH. (a) In the Zn-IBA−NADH−LADH complex (cyan), the ring is puckered in a boat conformation, whereas the ring in the Cd-DMSO−NADH−LADH complex (green) is puckered in a twisted boat conformation, with the C5 atom elevated above the plane of the ring. The twist is described as the shortest distance between the C5 atom and the C2−C3−C6 plane (12). (b) A $2mF_o − DF_c$ electron density map for the nicotinamide in the IBA complex at contour levels of 2σ (0.94 e/Å^3) and 3.5σ (1.57 e/Å^3). (c) A $2mF_o − DF_c$ electron density map for the nicotinamide in the DMSO complex at 2σ (0.97 e/Å^3) and 3.25σ (1.58 e/Å^3). A sketch of the electronic state is displayed below the ring. In the IBA complex pyridine ring, the electron density is evenly distributed around the ring, suggesting an aromatic distribution. In the DMSO complex pyridine ring, the electron density is localized, with increased density along the N1−C2 and C4−C5 bonds.

inhibitor has deactivated the cofactor to a localized and polarized distribution, provides further evidence that the twisted boat puckering of the pyridine ring mimics a transition state.

DISCUSSION

Structural Changes Resulting from the Substitution of Zinc with Cadmium. Replacement of zinc with other transition metals has an effect on the activity of the enzyme. It has been proposed that for most zinc-dependent enzymes, the metal acts as a Lewis acid by (de)protonating the substrate (32) and that the rate of activity should follow a trend in Lewis acidity of the metals. A correlation between the activity of cobalt-, nickel-, zinc-, and cadmium-substituted enzymes and the acidic properties of these metals was observed for aldehyde reduction in LADH (14). Cobalt is a

stronger Lewis acid than zinc, and the cobalt-substituted enzyme has 140% activity compared to the native enzyme. Cadmium is a much weaker Lewis acid than zinc, and the cadmium-substituted enzyme has only 2.5% of the activity of the native enzyme. Among the metals used in substitution, the electronic configuration of cadmium is most similar to that of zinc, and previous X-ray structures do not indicate substantial differences in metal coordination between the native and cadmium-substituted enzyme (33).

To validate the effect of the substitution of zinc with cadmium on the enzyme structure, a comparison between the ternary complexes of LADH with NADH and MPD with either zinc (1HET) or cadmium (1HEU) is made. Superimposition of Zn-MPD−NADH and Cd-MPD−NADH using all Cα atom coordinates gives a rmsd of 0.1 Å. Only minor differences (rmsd = 0.2 Å) are observed within the substrate

recognition loop in the vicinity of the noncatalytic Cd site, covering residues 116−120. This loop is rigidified in the Cd-substituted enzyme, whereas in the native enzyme, it occupies two alternate conformations.

One significant difference is found in the arrangement of the second coordination sphere (at a distance of ∼4.5 Å) of the metal center at the active site, which is occupied by D49, R369, and E68. In particular, E68 has attracted much interest since it is conserved in most MDRs and is buried deep inside the structure opposite the substrate binding side of the metal. Site-directed mutagenesis has established the importance of both D49 and E68 for catalysis in yeast alcohol dehydrogenase (34). Theoretical calculations have pointed to the possibility that E68 can act as inner sphere ligand without violating energetic principles or steric rules (35) and may facilitate ligand exchange processes at the substrate site. In one subunit of the Cd-MPD−LADH complex, the side chain of E68 occupies an alternate conformation that points the carboxyl oxygen toward the metal (Figure 5a,b). At an interatomic distance of 3.0 Å, there is no covalent bond between E68 and the cadmium ion. However, when the ellipsoid is displayed for the cadmium ion to cover 99% of its van der Waals volume, it is clear there is a perturbation caused by E68, which directs the motion of the metal between E68 and the substrate site (Figure 5b). The cysteine ligands C46 and C174 are positioned at either side of the metal near the center of the ellipsoid. The elongation of the ellipsoid of the cadmium ion is not observed in the complex structure with DMSO (Figure 5c). Clearly, the second conformation of E68 causes the elongation of the cadmium ellipsoid. The larger radius of the cadmium ion stabilizes the conformation of the E68 side chain in the proximity of the metal. The perturbed angular correlation of γ-ray measurements on ^{111}Cd indicated perturbation by a fifth ligand in the binary complex, and it was suggested this could be E68 (36). This is corroborated by the binary structure of human glutathione-dependent formaldehyde dehydrogenase (FDH) with NAD(H) (37), where the metal-bound water molecule is replaced with the glutamic acid as a metal ligand. In addition, structural and mutational studies on FDH indicated a critical role for E68 in the capture of substrates for catalysis (38).

Contribution of a Tautomeric Switch in Aldehyde Reduction. In the Zn-IBA−NADH structure, the IBA molecule forms a partial adduct with the NADH cofactor. A similar configuration was observed in the structure of LADH in complex with NAD$^+$ and pyrazole, where a pyrazole molecule is adducted to NAD$^+$ (39). Both compounds are strong but reversible inhibitors, and kinetic studies indicate they strengthen binding of the cofactor to the enzyme (15, 40). The fact that inhibition is reversible is reflected in the structure by the two conformations of the inhibitor. In *Drosophila* short chain alcohol dehydrogenase, formation of an adduct between a ketone and the NAD$^+$ cofactor leads to irreversible inhibition (41). In accordance, a series of ketone complex structures show complete conversion of the ketone into a compound adducted to the cofactor (42).

The IBA molecule is a substrate analogue of acetaldehyde, the product of ethanol oxidation. Acetaldehyde exists as a tautomer alternating between a keto form and an enol form. It seems feasible that a transition state occurs where the enol form binds to the metal while the carbonyl bond is weakened.
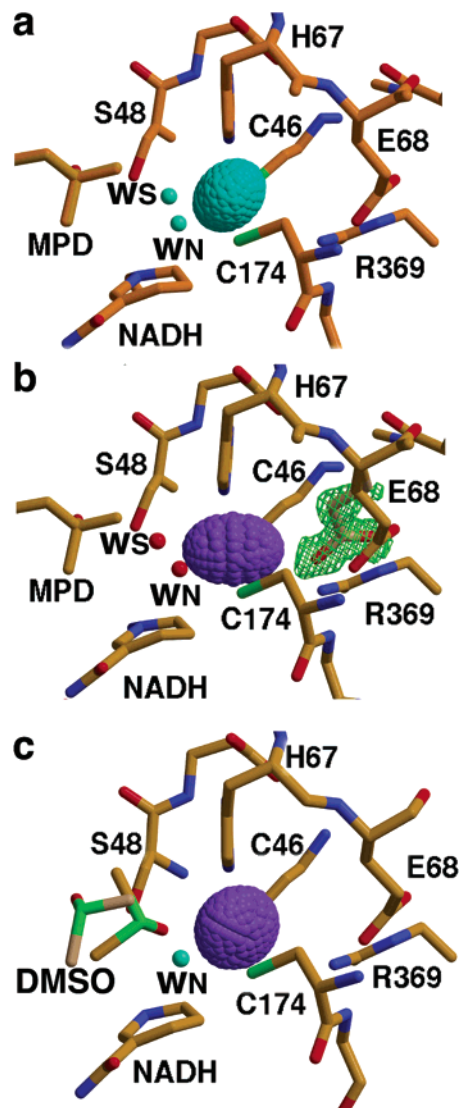

FIGURE 5: Comparison between the active sites of (a) native zinc, (b) cadmium-substituted NADH−LADH complex with MPD, and (c) cadmium-substituted NADH−LADH complex with DMSO. The metal ion is represented as an ellipsoid based on its anisotropic displacement parameter covering 99% of its volume. Active site residues are displayed as sticks and the two zinc-bound water/hydroxide molecules as spheres. The water occupying the substrate binding site is denoted WS, and the water molecule close to the nicotinamide is denoted WN. An omit map at 3σ (0.21 e/Å^3) is displayed in panel b for the alternate conformation of E68 that is near the metal ion.

A similar role for the enol form of aldehydes has been proposed to explain the formation of a NADH−ketone adduct in *Drosophila* short chain alcohol dehydrogenase (42).

Structural Evidence of a Coordination Shift at the Active Site. The Cd-DMSO−NADH structure provides a snapshot of the ternary LADH complex prior to the binding of the substrate analogue DMSO to the active site metal. The DMSO molecule is not yet bound to the metal yet is close enough to the active site to displace the hydroxide ion from the position that coincides with the inhibitor and/or substrate binding site (WS) to a position close to the NADH molecule (WN). This displacement causes a strong interaction between NADH and the hydroxide ion, which distorts the nicotinamide. This distortion could provide the transition energy needed for the transfer of a hydride from the NADH

molecule to the substrate. In concurrence, the displaced hydroxide ion forms hydrogen bonds with both the substrate analogue and S48, which is thought to provide the proton that completes the aldehyde reduction. This seems to be an ideal configuration for the proton relay system, where the hydroxide ion helps to attract a proton to the active site. The configuration in the active site of the Cd-DMSO−NADH−LADH structure shows how the metal-bound water molecule is displaced upon binding of the aldehyde substrate. The current structure does not resolve whether a transient pentacoordinate metal complex occurs. It remains to be seen whether the ligand coordination switch is followed by the complete dissociation of the metal-bound water molecule. In this scenario, there is no transient pentacoordinate metal complex and the current structure could represent the intermediate observed with spectroscopic methods. In case a transient pentacoordinate metal complex does occur, the water molecule may well reside close to the nicotinamide during the conversion of the substrate and return to the substrate position after the release of product. The complete repulsion of the water molecule from the active site is then an essential part of the inhibition process.

ACKNOWLEDGMENT

SUPPORTING INFORMATION AVAILABLE

Metal−ligand distances for subunits A and B (Table S1a) and angles between the active site metal and its ligands (Table S1b). This material is available free of charge via the Internet at http://pubs.acs.org.

REFERENCES

1. Jornvall, H., Nordling, E., and Persson, B. (2003) Multiplicity of eukaryotic ADH and other MDR forms, *Chem.-Biol. Interact. 143*, 255−261.

2. Voet, D., Voet, J. G., and Pratt, C. W. (2006) *Fundamentals of biochemistry: Life at the molecular level*, 2nd ed., Wiley, New York.

3. Brändén, C. I., Eklund, H., Nordstrom, B., Boiwe, T., Soderlund, G., Zeppezauer, E. S., Ohlsson, I., and Åkeson, Å (1973) Structure of liver alcohol dehydrogenase at 2.9-angstrom resolution, *Proc. Natl. Acad. Sci. U.S.A. 70*, 2439−2442.

4. Rossmann, M. G., Moras, D., and Olsen, K. W. (1974) Chemical and biological evolution of nucleotide-binding protein, *Nature 250*, 194−199.

5. Meijers, R., and Cedergren-Zeppezauer, E. S. (2004) Zn-dependent medium-chain dehydrogenases/reductases, in *Handbook of Metalloproteins* (Messerschmidt, A., Bode, W., and Cygler, M., Eds.) pp 5−33, John Wiley & Sons, Ltd., Chichester, U.K.

6. Pettersson, G. (1987) Liver alcohol dehydrogenase, *CRC Crit. Rev. Biochem. 21*, 349−389.

7. Cho, H., Ramaswamy, S., and Plapp, B. V. (1997) Flexibility of liver alcohol dehydrogenase in stereoselective binding of 3-butylthiolane 1-oxides, *Biochemistry 36*, 382−389.

8. Al-Karadaghi, S., Cedergren-Zeppezauer, E. S., Hovmöller, S., Petratos, K., Terry, H., and Wilson, K. S. (1994) Refined crystal structure of liver alcohol dehydrogenase-NADH complex at 1.8 Å resolution, *Acta Crystallogr. D50*, 793−807.

9. Eklund, H., and Brändén, C. I. (1987) Alcohol Dehydrogenase, in *Biological Macromolecules and Assemblies* (Jurnak, F. A., and McPherson, A., Eds.) Wiley, New York.

10. Makinen, M. W., Maret, W., and Yim, M. B. (1983) Neutral metal-bound water is the base catalyst in liver alcohol dehydrogenase, *Proc. Natl. Acad. Sci. U.S.A. 80*, 2584−2588.

11. Kleifeld, O., Frenkel, A., Martin, J. M., and Sagi, I. (2003) Active site electronic structure and dynamics during metalloenzyme catalysis, *Nat. Struct. Biol. 10*, 98−103.

12. Meijers, R., Morris, R. J., Adolph, H. W., Merli, A., Lamzin, V. S., and Cedergren-Zeppezauer, E. S. (2001) On the enzymatic activation of NADH, *J. Biol. Chem. 276*, 9316−9321.

13. Perlman, R. L., and Wolff, J. (1968) Dimethyl sulfoxide: An inhibitor of liver alcohol dehydrogenase, *Science 160*, 317−319.

14. Dunn, M. F., Dietrich, H., MacGibbon, A. K., Koerber, S. C., and Zeppezauer, M. (1982) Investigation of intermediates and transition states in the catalytic mechanisms of active site substituted cobalt(II), nickel(II), zinc(II), and cadmium(II) horse liver alcohol dehydrogenase, *Biochemistry 21*, 354−363.

15. Theorell, H., and McKinley-McKee, J. S. (1961) Liver alcohol dehyrogenase II. Equilibrium constants of binary and ternary complexes of enzyme, coenzyme and caprate, isobutyramide and imidazole, *Acta Chem. Scand. 15*, 1811−1833.

16. Hubatsch, I., Maurer, P., Engel, D., and Adolph, H. W. (1995) Preparation and characterization of isozymes and isoforms of horse liver alcohol dehydrogenase, *J. Chromatogr., A 711*, 105−112.

17. Maret, W., Andersson, I., Dietrich, H., Schneider-Bernlohr, H., Einarsson, R., and Zeppezauer, M. (1979) Site-specific substituted cobalt(II) horse liver alcohol dehydrogenases. Preparation and characterization in solution, crystalline and immobilized state, *Eur. J. Biochem. 98*, 501−512.

18. Bourne, P. E., Westbrook, J., and Berman, H. M. (2004) The Protein Data Bank and lessons in data management, *Briefings Bioinf. 5*, 23−30.

19. Otwinowski, Z., and Minor, W. (1997) Processing of X-ray diffraction data collected in oscillation mode, in *Methods in Enzymology* (Carter, C. W., and Sweet, R. M., Eds.) Academic Press, San Diego.

20. Schneider, T. R., and Sheldrick, G. M. (1997) SHELXL: High-resolution refinement, in *Methods in Enzymology* (Carter, C. W., and Sweet, R. M., Eds.) Academic Press, San Diego.

21. Murshudov, G. N., Vagin, A. A., Lebedev, A., Wilson, K. S., and Dodson, E. J. (1999) Efficient anisotropic refinement of macromolecular structures using FFT, *Acta Crystallogr. D55*, 247−255.

22. McRee, D. E. (1999) XtalView/Xfit: A versatile program for manipulating atomic coordinates and electron density, *J. Struct. Biol. 125*, 156−165.

23. Perrakis, A., Morris, R. J., and Lamzin, V. S. (1999) Automated protein model building combined with iterative structure refinement, *Nat. Struct. Biol. 6*, 458−463.

24. Winn, M. D. (2003) An overview of the CCP4 project in protein crystallography: An example of a collaborative project, *J. Synchrotron Radiat. 10*, 23−25.

25. Delano, W. L. (2002) *The Pymol Molecular Graphics System*, DeLano Scientific, San Carlos, CA.

26. Adolph, H. W., Zwart, P., Meijers, R., Hubatsch, I., Kiefer, M., Lamzin, V., and Cedergren-Zeppezauer, E. S. (2000) Structural basis for substrate specificity differences of horse liver alcohol dehydrogenase isozymes, *Biochemistry 39*, 12885−12897.

27. Eklund, H., Plapp, B. V., Samama, J. P., and Brändén, C. I. (1982) Binding of substrate in a ternary complex of horse liver alcohol dehydrogenase, *J. Biol. Chem. 257*, 14349−14358.

28. LeBrun, L. A., Park, D. H., Ramaswamy, S., and Plapp, B. V. (2004) Participation of histidine-51 in catalysis by horse liver alcohol dehydrogenase, *Biochemistry 43*, 3014−3026.

29. Kovaleva, E. G., and Plapp, B. V. (2005) Deprotonation of the Horse Liver Alcohol Dehydrogenase-NAD$^+$ Complex Controls Formation of the Ternary Complexes, *Biochemistry 44*, 12797−12808.

30. Eklund, H., Samama, J. P., Wallen, L., Brändén, C. I., Åkeson, Å., and Jones, T. A. (1981) Structure of a triclinic ternary complex of horse liver alcohol dehydrogenase at 2.9 Å resolution, *J. Mol. Biol. 146*, 561−587.

31. Ramaswamy, S., Scholze, M., and Plapp, B. V. (1997) Binding of formamides to liver alcohol dehydrogenase, *Biochemistry 36*, 3522−3527.

32. Coleman, J. E. (1998) Zinc enzymes, *Curr. Opin. Chem. Biol. 2*, 222−234.

33. Schneider, G., Cedergren-Zeppezauer, E. S., Knight, S., Eklund, H., and Zeppezauer, M. (1985) Active site specific cadmium(II)-substituted horse liver alcohol dehydrogenase: Crystal structures of the free enzyme, its binary complex with NADH, and the

ternary complex with NADH and bound p-bromobenzyl alcohol, *Biochemistry 24*, 7503−7510.

34. Ganzhorn, A. J., and Plapp, B. V. (1988) Carboxyl groups near the active site zinc contribute to catalysis in yeast alcohol dehydrogenase, *J. Biol. Chem. 263*, 5446−5454.

35. Ryde, U. (1995) On the role of Glu-68 in alcohol dehydrogenase, *Protein Sci. 4*, 1124−1132.

36. Hemmingsen, L., Bauer, R., Bjerrum, M. J., Zeppezauer, M., Adolph, H. W., Formicka, G., and Cedergren-Zeppezauer, E. S. (1995) Cd-substituted horse liver alcohol dehydrogenase: Catalytic site metal coordination geometry and protein conformation, *Biochemistry 34*, 7145−7153.

37. Yang, Z. N., Bosron, W. F., and Hurley, T. D. (1997) Structure of human alcohol dehydrogenase: A glutathione-dependent formaldehyde dehydrogenase, *J. Mol. Biol. 265*, 330−343.

38. Sanghani, P. C., Davis, W. I., Zhai, L., and Robinson, H. (2006) Structure-Function Relationships in Human Glutathione-Dependent Formaldehyde Dehydrogenase. Role of Glu-67 and Arg-368 in the Catalytic Mechanism, *Biochemistry 45*, 4819−4830.

39. Rubach, J. K., Ramaswamy, S., and Plapp, B. V. (2001) Contributions of valine-292 in the nicotinamide binding site of liver alcohol dehydrogenase and dynamics to catalysis, *Biochemistry 40*, 12686−12694.

40. Li, T. K., and Theorell, H. (1969) Human liver alcohol dehydrogenase: Inhibition by pyrazole and pyrazole analogs, *Acta Chem. Scand. 23*, 892−902.

41. Winberg, J. O., and McKinley-McKee, J. S. (1988) *Drosophila melanogaster* alcohol dehydrogenase. Biochemical properties of the NAD$^+$-plus-acetone-induced isoenzyme conversion, *Biochem. J. 251*, 223−227.

42. Benach, J., Atrian, S., Gonzalez-Duarte, R., and Ladenstein, R. (1999) The catalytic reaction and inhibition mechanism of *Drosophila* alcohol dehydrogenase: Observation of an enzyme-bound NAD-ketone adduct at 1.4 Å resolution by X-ray crystallography, *J. Mol. Biol. 289*, 335−355.

43. Cruickshank, D. W. (1999) Remarks about protein structure precision, *Acta Crystallogr. D55*, 583−601.

BI6023594